

Quantitative Flow Visualization

Toward a Comprehensive Flow Diagnostic Tool

MORY GHARIB, FRANCISCO PEREIRA, DANA DABIRI,
AND DARIUS MODARRESS

*Graduate Aeronautical Laboratory, California Institute of Technology,
Pasadena, California, USA*

ABSTRACT: Quantitative flow visualization has many roots and has taken several approaches. The advent of digital image processing has made it practical to extract useful information from every kind of flow image. In a direct approach, the image intensity or color (wavelength or frequency) can be used as an indication of concentration, density and temperature field, or gradients of these scalar fields in the flow.¹ For whole-field velocity measurement, the method of choice for experimental fluid mechanics has been digital particle image velocimetry (DPIV). This paper presents a novel approach to extend the DPIV technique from a planar method to a full three-dimensional volume mapping technique.

KEYWORDS: imaging; visualization; PIV; DPIV; diagnostics

INTRODUCTION

In general, the optical flow or the motion of intensity fields can be obtained through a time sequence of images.² For example, the motion of patterns generated by dye, clouds, or particles can be used to obtain such a time sequence. The main problem with using a continuous-intensity pattern, generated by scalar fields (e.g., dye patterns), is that it must be fully resolved (space/time) and contain intensity variations at all scales, before mean and turbulent velocity information can be obtained.³ In this respect, the discrete nature of images generated by seeding particles has made particle tracking the method of choice for the entire velocimetry field. Various methods, such as individual tracking of particles or statistical techniques, can be used to obtain the displacement information and subsequently the velocity information. The spatial resolution of this method depends on the number density of the particles.

The *particle image velocimetry* (PIV) technique follows a group of particles through statistical correlation of sampled windows of the image field.⁴ This scheme removes the problem of identifying individual particles, which is often associated with tedious operations and large errors in the detection of particle pairs. In terms of the spatial resolution, the velocity obtained at each window represents the average velocity of the group of particles within the window. The interrogating window in PIV is the equivalent of a grid cell in CFD. Development of the video-based digital

Address for correspondence: Mory Gharib, Ph.D., Graduate Aeronautical Laboratory, California Institute of Technology, Pasadena, CA, USA.
mory@caltech.edu

version of PIV, known as DPIV,^{5,6} resulted directly from advances in charge coupled device (CCD) technology and fast, computer-based, image processing systems.

The capability of whole field measurement techniques in providing velocity vector or scalar field information in a format compatible with CFD calculations has made a major impact in defining common grounds for designing new approaches toward resolving the turbulent and two-phase flow problem. Such common grounds are difficult or impossible to define by using methods, such as LDV or hot wire anemometry, that do not address the global Lagrangian and the temporal nature of complex flows.

DPIV can be utilized to obtain three components of the velocity field. However, this extension of DPIV is limited to a few planes and cannot address the full dimensionality of turbulent flow with current video technology. *Holographic PIV techniques* are more suitable for obtaining three-dimensional (3D) distributions of the velocity vector field.⁷ The photographic nature of holographic PIV techniques limits their ability to address the temporal dynamics of turbulent flows. Recent advances in 3D video-based particle tracking techniques have removed some of these shortcomings.⁸ However, complexities involved in the optics, calibration, and image processing of multiple cameras and images severely limits the wide range application of multiple-camera stereo techniques.

An emerging technology that has a good potential for resolving difficulties associated with the aforementioned flow mapping techniques is the *method of defocusing imaging*.⁹ *Defocusing digital particle image velocimetry* (DDPIV) is the natural extension of planar PIV techniques to a third spatial dimension. This method has shown great potential for two-phase flow studies.¹⁰

THE DEFOCUSING CONCEPT

The foundations of the defocusing concept were established in an early paper by Willert and Gharib.⁹ We report here the most important aspects in a revised form. For clarity, we use the term *particle* when referring either to a solid particle or to a bubble.

A typical two-dimensional imaging system, consisting of a convergent lens and an aperture, is represented in FIGURE 1 to help describe the DDPIV technique. FIGURE 1A exhibits a point A , located on the object plane (or reference plane), and a point B placed in between this plane and the lens system. Point A appears focused in A' , on the image plane (or sensor plane), whereas B is projected as a blurred image B' . The DDPIV technique uses a mask, with two or more apertures shifted away from the optical axis, to obtain multiple images from each scattering source, as shown in FIGURE 1B. The image shift b on the image plane, caused by these off-axis apertures, is related to the depth location of the source points, whereas the scattered light intensity combined with the blurredness is used to recover the size information.

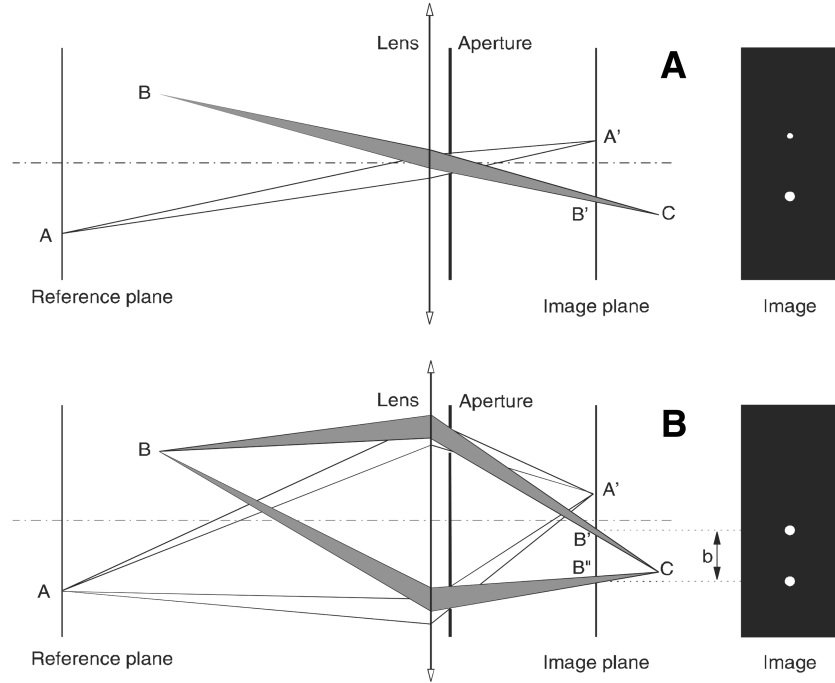


FIGURE 1. The defocusing principle: (A) standard g system, (B) defocusing arrangement.

GEOMETRIC ANALYSIS

A simplified geometric model of a two-aperture defocusing optical arrangement is represented in FIGURE 2. The interrogation domain is defined as a cube of side length a , thus, a square in the plane. The back face of this cube is on the reference plane, which is placed at a distance L from the lens plane. Let d be the distance between apertures, f the focal length of the converging lens, and l the distance from the lens to the image plane. The image plane is materialized by a photosensor (e.g., CCD) of height h . The physical space is attached to a coordinate system originating in the lens plane, with the Z -axis on the optical axis of the system. Coordinates in the physical space are designated (X, Y, Z) . The image coordinate system is simply the Z -translation of the physical system onto the sensor plane, that is, at $Z = -1$. The coordinates of a pixel on the imaging sensor are given by the pair (x, y) . Point $P(X, Y, Z)$ represents a light scattering source, such as particle, bubble, or a point-like dot. For $Z \neq L$, P is projected onto points $P'(x', y')$ and $P''(x'', y'')$, separated by a distance b .

The coordinates (x', y') and (x'', y'') of the images P' and P'' of $P(X, Y, Z)$ in the image plane are given by the following relations:

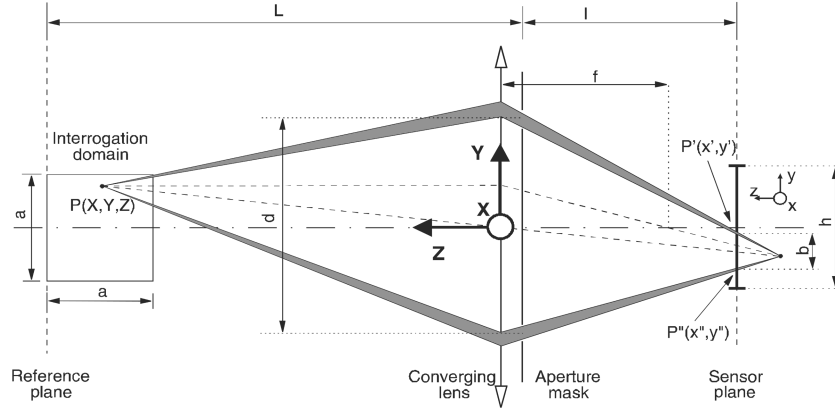


FIGURE 2. Simplified defocusing optical method.

$$\begin{cases} x' = x'' = -ML\frac{X}{Z} \\ y' = \frac{M}{2Z}[d(L-Z) - 2LY] \\ y'' = \frac{M}{2Z}[-d(L-Z) - 2LY] \end{cases} \quad (1)$$

where M is the optical magnification provided by the lens equation.

The image separation vector \mathbf{b} represents the distance between the images P' and P'' . The norm is, therefore, given by

$$b = \frac{Md}{Z}(L-Z) = \frac{1}{K}\left(\frac{1}{Z} - \frac{1}{L}\right) \quad \text{with } K = \frac{1}{MdL}. \quad (2)$$

Equation (2) demonstrates the extreme simplicity of the defocusing concept, which, of course, is valuable in terms of computational implementation and processing speed. In purely geometric terms, the image separation b is independent of the in-plane coordinates X and Y . Likewise, the pinhole diameter has no bearing on b and is only responsible for the amount of blurredness of any given particle image. For our prototype instrument, we use three pinholes, arranged in a triangular pattern. This configuration, shown in FIGURE 3, exhibits a flipping triangle when P moves across the reference plane and requires straightforward and fast image processing routines.

The sensitivity of the system—its ability to detect small changes of the particle location—can be evaluated through the separation gradient

$$\frac{\partial b}{\partial Z} = -\frac{1}{KZ^2}. \quad (3)$$

The coordinates of P in the global coordinate system are derived from the image coordinates of the projections P' and P'' , see (1),

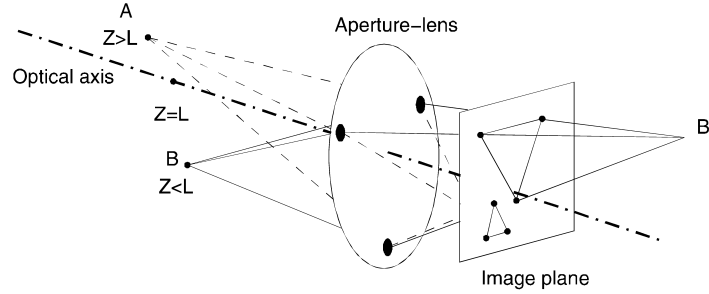


FIGURE 3. Three-aperture arrangement.

$$\begin{cases} X = -\frac{x_0 Z}{ML} & \text{with } x_0 = \frac{x' + x''}{2} \\ Y = -\frac{y_0 Z}{ML} & \text{with } y_0 = \frac{y' + y''}{2} \\ Z = \frac{1}{1/L + Kb} \end{cases} \quad (4)$$

Assuming that the apertures are equidistant from the origin of the coordinate system, the image point defined by (x_0, y_0) is the image of the particle if there were a single aperture at the origin.

A camera system has been designed and fabricated based on this concept. Specific characteristics of the instrument can be found in the paper by Pereira *et al.*¹⁰ The velocity vector field is obtained by local spatial cross-correlation between small volume elements (*voxels*) containing particles observed at two time steps, as shown and discussed by Pereira *et al.*¹⁰

APPLICATIONS

Two-Blade Model Propeller

A propeller was immersed in a water tank. The rotation speed was 12 rps, corresponding to a tangential velocity of 2.52 msec^{-1} at the tip of the blades. A bubble generator, placed below the propeller, produced a dense stream of rising submillimeter air bubbles. The velocity field was obtained by phase averaging.

A 3D velocity field was obtained after averaging and outlier correction. Mass-less particles were then artificially injected into the mean velocity data set, in a radial arrangement and one diameter upstream from the propeller. Paths of bubbles were determined, providing a unique insight into this complex flow, as shown in FIGURE 4. The gray level in this figure relates to the local measured velocity amplitude. The velocity reached a maximum of 2.49 msec^{-1} in the outer region of the propeller, matching closely the blade tip tangential velocity.

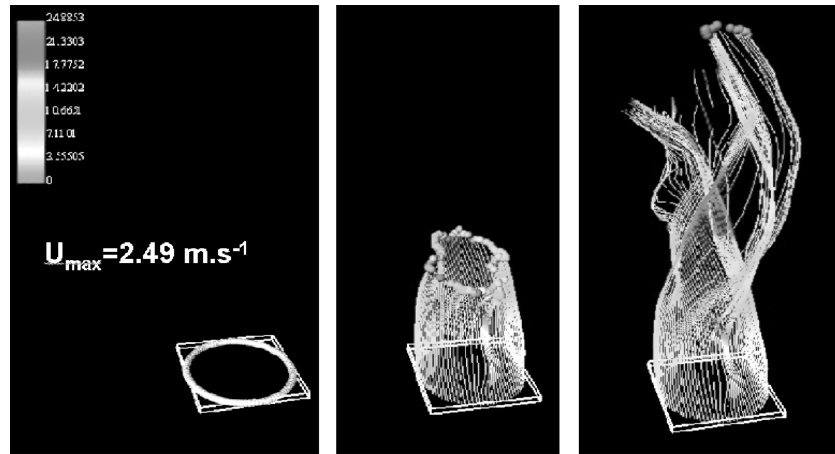


FIGURE 4. Path lines of bubbles around the propeller.

The bubble mean radius along the Y vertical axis of the flow (rotation axis of the propeller) is displayed in FIGURE 5. The mean radius increases almost linearly to nearly 325 μm at $Y \approx 30\text{mm}$, where the propeller was located. After the bubbles pass the immediate vicinity of the propeller, the radius is found to follow the opposite trend, decreasing to about 200 μm . The growth of bubbles is partly due, but to a very small extent, to the decrease of the static pressure with increasing Y . In fact, bubbles experience first the low pressure in the suction side of the propeller before getting into the high-pressure region where they collapse. Included in FIGURE 5 are the histograms, calculated by taking the same volume below and above $Y = 30\text{mm}$. The histogram peak follows the trend outlined previously and due to the pressure variations.

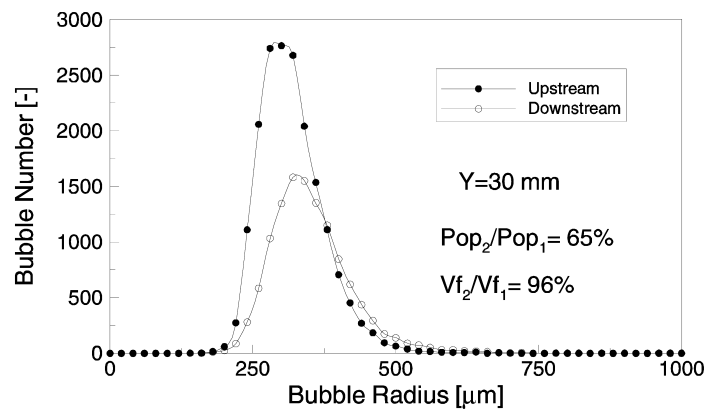


FIGURE 5. Size distribution upstream and downstream, $Y = 30\text{cm}$.

The ratio of the upstream to the downstream populations is 65%. However, the ratio of the respective void fractions is close to 100%. These observations indicate that coalescence of bubbles is the main mechanism acting here, although breakup may occur in the propeller region.

Three-Blade Boat Propeller

The three-blade propeller had a similar configuration to the two-blade propeller discussed above. The propeller was rotated at 12 Hz. The velocity field, represented in FIGURE 6 was obtained by phase-averaging a sequence of 50 instantaneous velocity fields. Spurious vectors can be seen on the borders of the interrogation domain. A slice in the velocity field (see FIGURE 7) displays the high speed jet core along the downstream section of the propeller axis. However, the isovelocity contours, displayed in the same figure, show a viscous wake that appears as a velocity defect due to the merging of the two boundary layers from the blades. A slight contraction of the slipstream could also be detected. The wake was found to rapidly fade into the bulk flow.

SUMMARY

In this paper we seek to present some recent advances in the field of quantitative visualization. Only techniques that can provide time resolved, 3D velocity vector

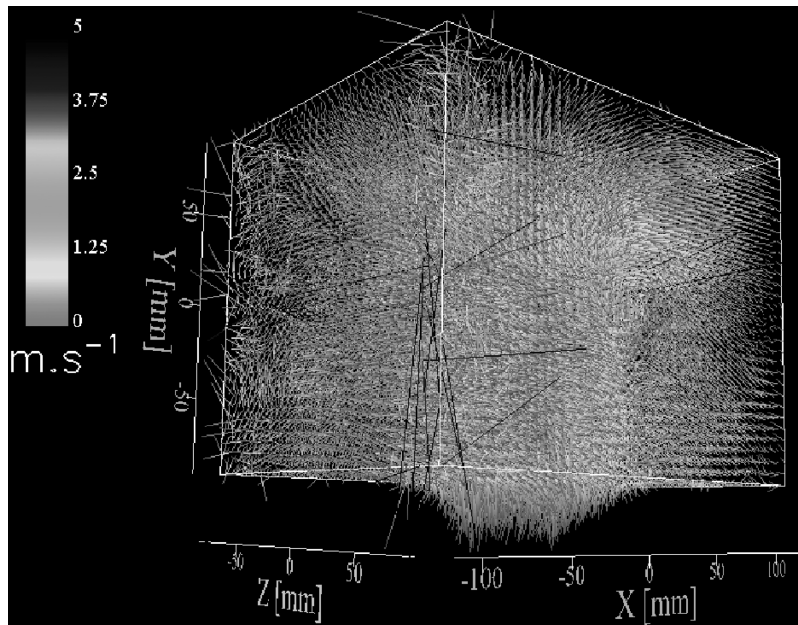


FIGURE 6. Velocity field, $200 \times 200 \times 400 \text{ mm}^3$, 72,963 vectors ($33 \times 33 \times 67$ voxels).

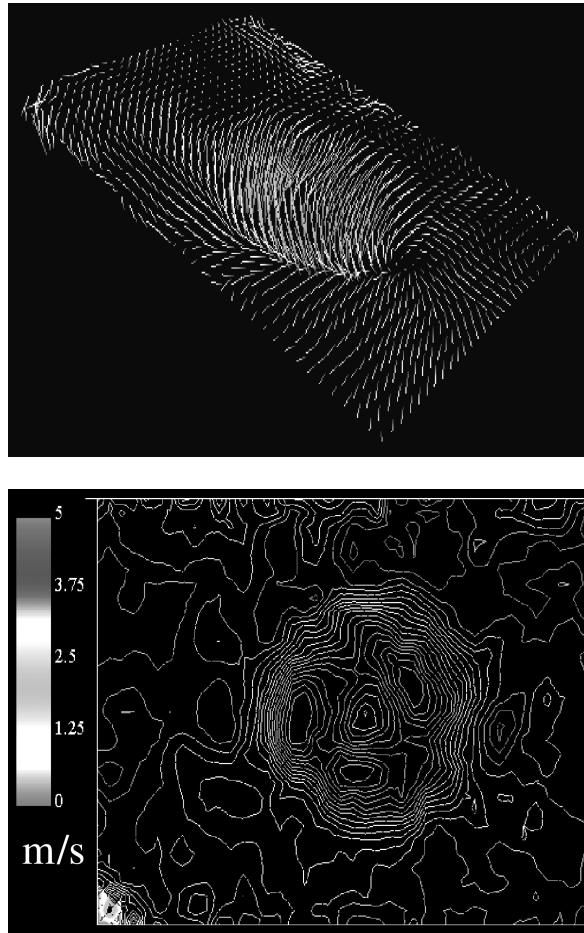


FIGURE 7. Top, velocity cross-section (downstream region, 0.5 diameter); bottom, corresponding isovelocity contour.

fields can offer hope in defining better common grounds with CFD. In this respect the novel method of DDPIV shows excellent potential in providing quantitative flow information comparable with that of CFD.

ACKNOWLEDGMENTS

This research was supported by the Office of Naval Research (Contract N000140010110). Defocusing digital particle image velocimetry (DDPIV) technology is protected under a U.S. patent through the California Institute of Technology.

REFERENCES

1. MERZKIRCH, W. 1987. Flow Visualization. Academic Press.
2. SINGH, A. 1991, Optic flow computation. IEEE, Computer Society Press.
3. PEARLSTEIN, A.J. & B. CARPENTER. 1995. On the determination of solenoidal or compressible velocity fields from measurements of passive and reactive scalars. *Phys. Fluids* **7**(4): 754–763.
4. ADRIAN, R.J. 1991. Particle-imaging techniques for experimental fluid mechanics. *Annu. Rev. Fluid Mechan.* **23**: 261–304.
5. WILLERT, C. & M. GHARIB. 1991. Digital particle image velocimetry. *Exp. Fluids* **10**: 181–183.
6. WESTERWEEL, J. 1993. Digital Image Velocimetry: Theory and Application. Delft UP, Delft, the Netherlands.
7. BARNHART, D.H., R.J. ADRIAN & G.C. PAPEN. 1994. Phase-conjugate holographic system for high resolution PIV. *Appl. Optics* **3**(30): 7159–7170.
8. KASAGI, N. & Y. SATA. 1992. Recent development in three-dimensional particle tracking velocimetry. *Proc. of Flow Visualization Conference VI*, Yokohama, Japan.
9. WILLERT C.E. & M. GHARIB. 1992. Three-dimensional particle imaging with a single camera. *Exp. Fluids* **12**: 353–358.
10. PEREIRA, F., M. GHARIB, M. MODARRESS & D. DABIRI. 2000. Defocusing digital particle imaging velocimetry: A 3-component 3-D DPIV measurement technique, application to bubbly flows. *Exp. Fluids* **29**: S78–S84.